BWB Aerodynamic Analysis and Redesign

16.100 Final Project

Scarlett Koller, Johannes Norheim, Berk Öztürk, Isabel Vallina García, Jamie Voros

December 10, 2014

Work Breakdown

Scarlett Koller

Carried out mount drag corrections for WBWT data, analytic wave drag estimation for original and modified BWB, aerodynamic analysis research, BWB redesign - planning and execution in AVL, partial write-up of report, provided snacks.
Time: 35 hours

Johannes Norheim

Generated drag polars in XFoil for airfoil sections, added drag polars into BWB AVL file, generated drag polars for full BWB in WBWT conditions using AVL, plotted corrected WBWT data in MATLAB, compared predictions with measured WBWT data, created MATLAB code to automate BWB geometry modification, provided snacks.
Time: 50 hours

Berk Öztürk

Generated drag polars in XFoil for airfoil sections, added drag polars into BWB AVL file, created MATLAB code to automate BWB geometry modification, BWB redesign - planning and execution in AVL, produced Trefftz plots for cruise analysis of original and redesigned BWB.
Time: 45 hours

Isabel Vallina García

Carried out wind tunnel corrections for WBWT data, analytic wave drag estimation for original and modified BWB, aerodynamic analysis research, write-up for wind tunnel corrections, wave drag estimation and bibliography.
Time: 35 hours

Jamie Voros

Carried out approach, stall, and cruise analysis of both original and redesigned BWB, general write-up and editing of report, created report layout and design, produced Trefftz plots for approach and stall analyses as well as all graphics and renders, provided snacks.
Time: 35 hours

1 Introduction

This project describes the steps taken to analyze the aerodynamic properties of the Boeing-designed Blended Wing Body (BWB), and to redesign the BWB for improved static stability at cruise, approach and stall conditions, while avoiding any significant drag penalties. Our redesign makes use of geometric twist, sweep, and a modified chord distribution in order to achieve a minimum of 5% pitch stability margin, while only incurring a drag penalty of 9%. We accomplished this by running comparisons between the AVL model of the BWB and the data collected in the Wright Brothers Wind Tunnel using a 1/47 scale model and implementing design changes in AVL.

2 Wind tunnel comparison: Nominal geometry

2.1 Wind tunnel walls and Mount mechanism corrections

Before conducting our analysis of the wind tunnel data, it was necessary to correct this data to account for the impact of the walls and the mount on the measured lift and drag.
First, to account for the impact on drag from the mount, we determined the drag on the elliptical pitch adjustment rod, cylindrical mount rod, and flat plate sting at the different operating velocities (50 and 100mph).
We assumed that all mount components were in a uniform free-stream with the same velocity as that set by the wind tunnel. We found the sectional drag coefficient of the cylindrical and elliptical rods using the Hoerner plots provided and the Reynolds number of each component in the free-stream.
We also used the Blasius Boundary Layer solution to estimate the skin friction drag on the sting, modeled as an infinitesimally thin plate. We determined that this drag was less than 1% of the drag on the other mount components, and therefore deemed it negligible for our purposes.
The Reynolds numbers of all the components were subcritical, giving us sectional drag coefficients of 0.6 for the elliptical rod and 0.9 for the cylindrical rod, according to the Hoerner plot.

$$D = \frac{1}{2}\rho_\infty U_\infty^2 S_{ref} C_D$$

Here, $C_D = c_d$ as neither rod is swept nor tapered. Using the frontal area of each rod as the reference area, we obtained values for the drag on each rod at both 50 and 100mph. We added the two drags to obtain the total mount drag for both operating velocities.

$$D_{50} = 0.638\text{lbs}$$

$$D_{100} = 2.55\text{lbs}$$

We then accounted for the impact on drag of the wind tunnel walls by implementing the method of images. For a fixed lift with a constant circulation, the image system causes an upwash which effectively increases the angle of attack. This net angle may be evaluated by adding the angle of attack induced by the upwash of the image system to the angle of attack of the model in the tunnel. An additional effect is a decrease in the induced drag relative to free-stream flight. The corrected drag coefficient is that of the tunnel plus the change caused by the image system; which may be found by multiplying the lift coefficient by the change in the effective angle of attack. We thus had to evaluate the change in the angle of attack for each of the data points provided. This was done using the given relationship:

$$\Delta\alpha_i = \delta\frac{S}{C}C_L$$

Where S is the reference area, C is the tunnel cross sectional area, and C_L is the lift coefficient. $\delta = 0.104$, a factor which depends on the tunnel and model geometry, determined using Figure 10.28 in the project briefing.
In order to determine the corrected drag we subtracted the drag caused by the mount from the given drag for each data point. This procedure was followed for both the 50mph and the 100mph cases.

2.2 AVL prediction

AVL makes the assumptions of an inviscid, incompressible flow, and in terms of drag, will only predict the induced drag generated by the scaled BWB. The lift coefficients would be expected match fairly well, but the drag will be largely underestimated due to the lack of a viscous and pressure drag predictions, especially at lower Reynolds numbers. In order to predict for viscous drag, we used AVL's built in parabolic drag model taking three points from a predefined drag polar. This was achieved by running XFOIL at a range of angles of attack and extrapolating the polar from three points. We then update the AVL files and run them to generate the requested comparisons. This process is repeated for both wind-tunnel readings of 50mph and 100mph. The diagram below depicts this process:

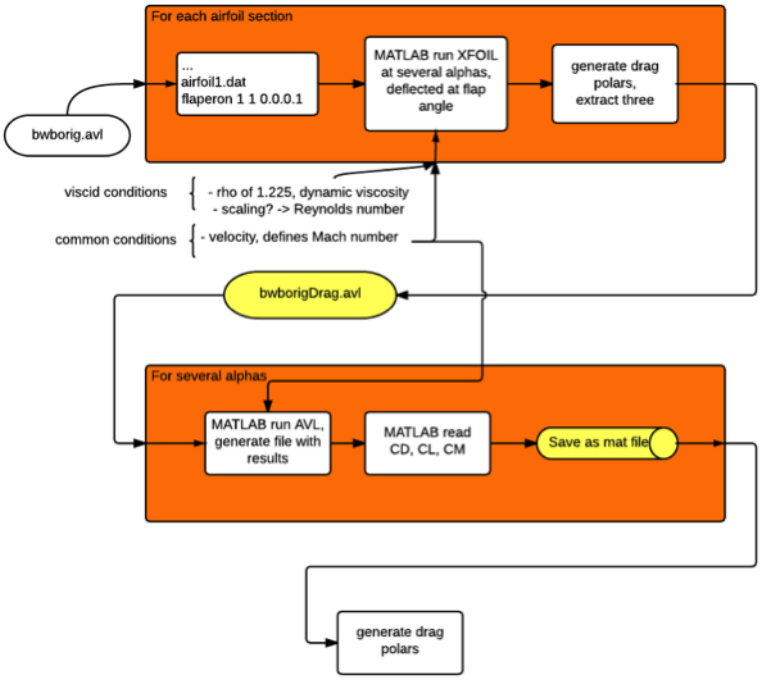

Figure 1: Process Diagram

2.3 Parabolic drag profile

The full process was programmatically done in MATLAB; the bwborig.avl file was parsed to retrieve the name of all the airfoil .dat files, which were then run through XFOIL to generate the sectional drag polars. In order to get a large enough range of angles of attack each of the 14 airfoils were run from -6 to +5 degrees at 0.25 degrees of increment. AVL takes as input three points, two which should be at the upper and lower boundary of the C_D, and one which should be at minimal C_D. It then makes a parabolic model, assuming the C_D minimal point is tangent to a parabola, and that the other two points bound the outer edges of the parabola. This can be verified in AVL source code in the file named cdcl.f.

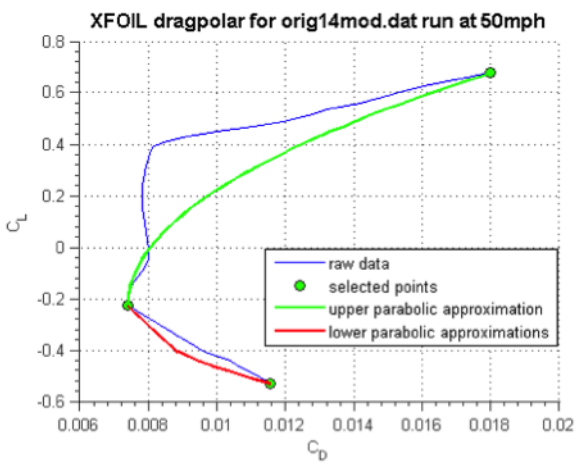

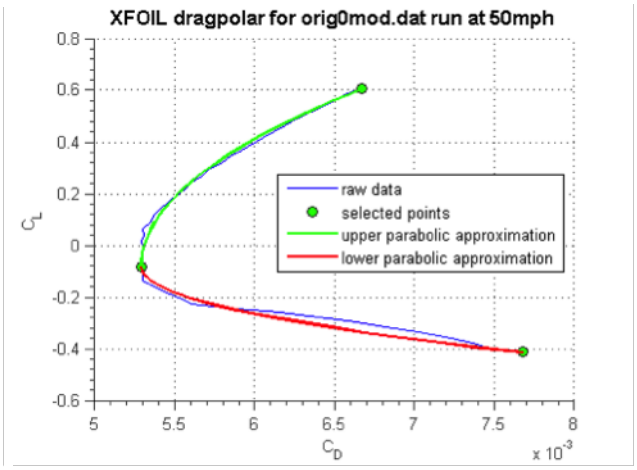

Figures 2 & 3: Fairly Poor Approximation at tip & Very Good Parabolic Approximation at Root

As the pictures above depict, the three point parabolic approximation will have different levels of accuracy depending on the airfoil section simulated. At the wingtip supercritical airfoil sections the approximation becomes very poor at higher angles of attack, so we therefore expect to see more significant differences between the corrected wind tunnel data and the AVL predictions for drag.

2.4 AVL wind tunnel data comparisons

The data recorded was sampled at two wind tunnel speeds: 50mph and 100mph. This means that the incompressible flow assumption holds. However, using the mean chord of the scaled BWB, we get Reynolds numbers of 305,000 and 610,000. For the first condition the Reynolds number will certainly be too low for inviscid assumptions to hold. We can see this effect in the following graphs of CL vs alpha for both cases:

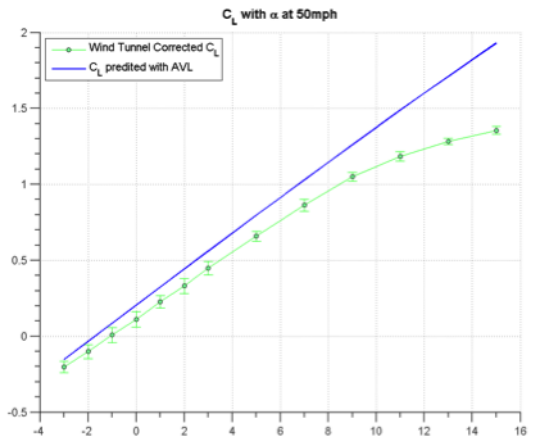

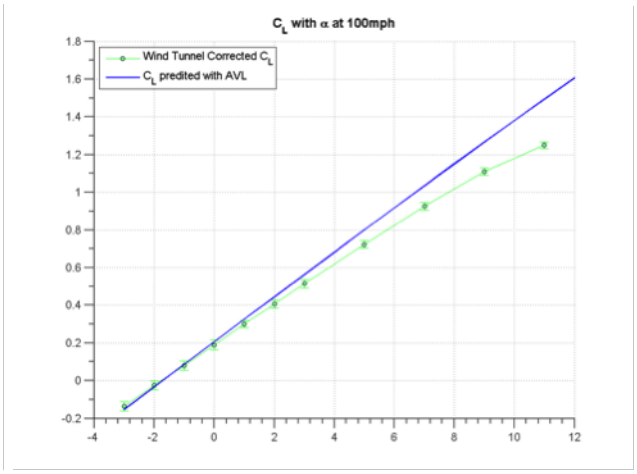

Figures 4 & 5: C_L Estimated Analytically and from Wind Tunnel results for 50mph & 100mph

In the first case, C_L is always off by a certain constant, while in the second case both the data and the prediction overlap fairly well, indicating small errors for small angles of attack. We also observe that the AVL prediction's linear behavior breaks down at larger angles, mostly likely due to separated flow.

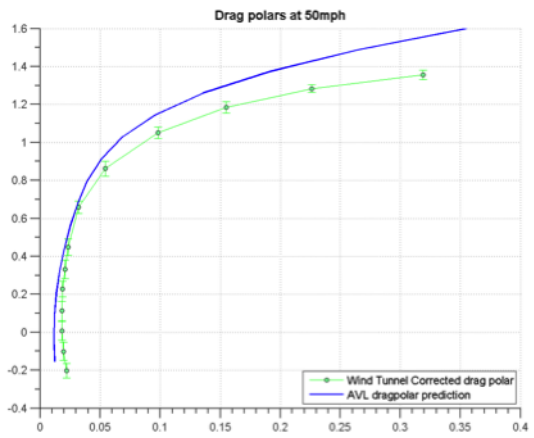

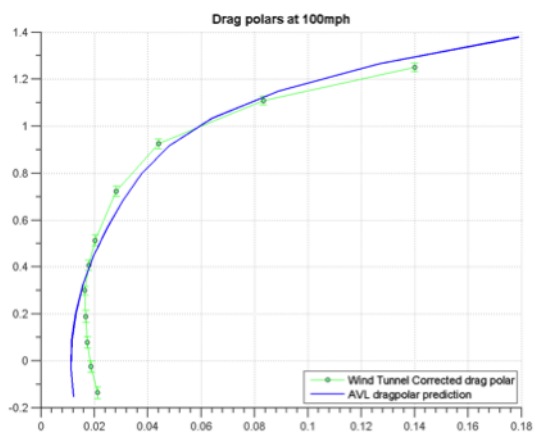

Figures 6 & 7: Drag Polars for BWB at 50mph & 100mph

Similarly, we observe an overlap in the drag polars which is fairly accurately depicted for small angles(close to zero), and diverges for larger or smaller angles. The better approximation in lift for the 100mph regime also accounts for the better accuracy of the drag polar at higher speeds.

2.5 Moment coefficients

We are interested in computing the moments about the aerodynamic center in order to check whether our predictions match the data. We are again restricted by low Reynolds flow data, and CM being a second order value we could expect to see slightly different values in tunnel From the wind tunnel we gather $C_{M,nose,tunnel}$, x_{cp} and $C_{L,tunnel}$. We can derive $C_{M,ac,tunnel}$ through the following formula: $C_{M,ac,tunnel} = (-x_{cp} + \frac{x_{np}}{c_{mac}})C_{L,tunnel} + C_{M,nose,tunnel}$
From AVLs prediction we derive $C_{M,ac,AVL}$ as follows:

$$C_{M,ac,AVL} = -\frac{x_{np}}{c_{mac}} + \frac{C_M}{C_L})C_L + C_M$$

Surprisingly enough the data seems to agree very well, and even better at lower Reynolds number. We are not so sure what could be causing this.

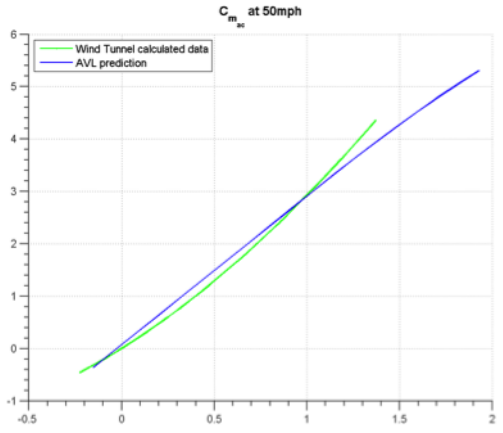

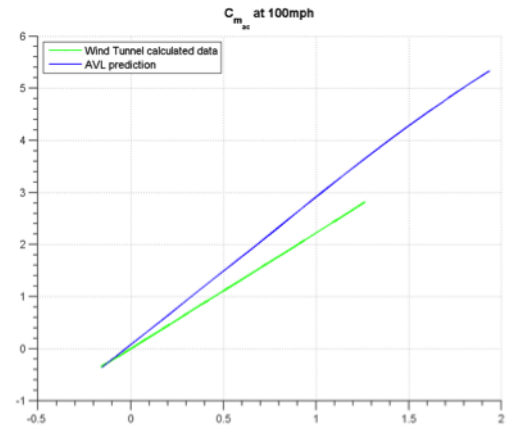

Figures 8 & 9: C_m plots for BWB at 50mph & 100mph

3 Cruise Analysis: Nominal Geometry

3.1 Drag and Lift-to-Drag Ratio Estimation

In order to estimate the wave drag, we consulted a number of papers published on aerodynamic analysis in transonic regimes, and used our references to develop a method of estimating wave drag analytically. We also attempted to make use of the availability of MSES on Athena computers. Unfortunately due to time constraints we were unable to go through a more accurate, complete transonic drag analysis through MSES.

To evaluate the wave drag on our swept wing in the transonic flow regime ($M = 0.8$), we used the Korn equation. This was initially used to estimate the divergence Mach number, M_{DD}, as a function of an airfoil technology factor κ_A, the thickness-to-chord ratio $\frac{t}{c}$, the lift coefficient c_l and the mid chord sweep angle $\Lambda_{0.5}$. The following relationship was used:

$$M_{DD}\cos\Lambda_{0.5} + \frac{C_L}{10\cos^2\Lambda_{0.5}} + \frac{t/c}{\cos\Lambda_{0.5}} = \kappa_A$$

The technology factor, κ_A, has a value of 0.87 for conventional subcritical airfoils and of 0.95 for supercritical airfoils. In our case, sections 1-7, the wing center, are subcritical whilst sections 8-14, the wing ends, are supercritical; thus, an average value of $\kappa_A = 0.9$ was used. The wing was approximated to have a triangular shape for simplicity, and this allowed us to approximate the sweep angle as 26.6 degrees. We estimated the thickness to chord ratio as 0.15. These approximations give a highly approximate value for wave drag, which we determined was a reasonable estimate to use to calculate drag in cruise conditions.

$$M_{DD} = 0.7548$$

$$M_{crit} = M_{DD} - (\frac{0.1}{80})^{1/3} = 0.647$$

$$C_{D_{wave}} = 20(M - M_{crit})^4 = 20(0.8 - 0.647)^4 = 0.01$$

In order to estimate the pressure drag and induced drag, AVL was used in the following fashion; first C_l was found analytically and then used in combination with the given Mach number to obtain these estimates directly from AVL.

Since $L = W$, at 35, 000 feet, $\rho_\infty = 0.381 kg/m^3 = 7.38 \times 10^{-4} sl/ft^3$ and U_{cruise} in ft/s use $a = 969$ ft/s. Using:

$$q_{cruise} = 0.5\rho_\infty U_{cruise}^2 = 222\text{lbs}/ft^2$$

$$\text{Weight} = W = W_{empty} + W_{payload} + W_{fuel} = 800,000\text{lbs}$$

C_L was found as is given below.

$$C_L = \frac{\text{Weight}}{q \cdot S_{ref}} = 0.460$$

With this C_L and the given Mach number of 0.8, AVL was used to find the following estimates for C_D and C_{D_i}. (Note that the AVL runs were performed at a Mach number of 0 since the compressible flow approximations that AVL can make are not accurate in the transonic regime).

$$C_D = 0.00976$$

$$C_{D_i} = 0.00988$$

A final estimate for the total $C_{D_{tot}}$ was made by simply summing these three components:

$$C_{D_{tot}} = 0.0296$$

The lift to drag ratio is defined as C_L/C_D:

$$\frac{L}{D} = 15.5$$

From this relation we can express the drag:

$$D = C_D q S_{ref} = 51,800\text{lbs}$$

This is a sensible and sustainable value; the three engines can provide up to 100, 000 lbs force together at any one time.

3.2 Stability Margin Calculations

With the aforementioned C_L and given Mach number at cruise, AVL was used to determine x_{ac} and x_{cp} and, therefore, the static margin. Given that AVL gives us C_M at $x = 0$, the center of pressure must be C_M/C_L since the moment of the center of pressure is zero. Additionally since the aircraft is tailless, the assumption that x_{np} and x_{ac} are equivalent was made.

$$\frac{x_{ac}}{c_{mac}} = \frac{x_{np}}{c_{mac}} = 2.78$$

$$\frac{x_{cp}}{c_{mac}} = \frac{|C_M|}{|C_L|} = 3.05$$

This gives a stability margin of -0.269, which is unstable.

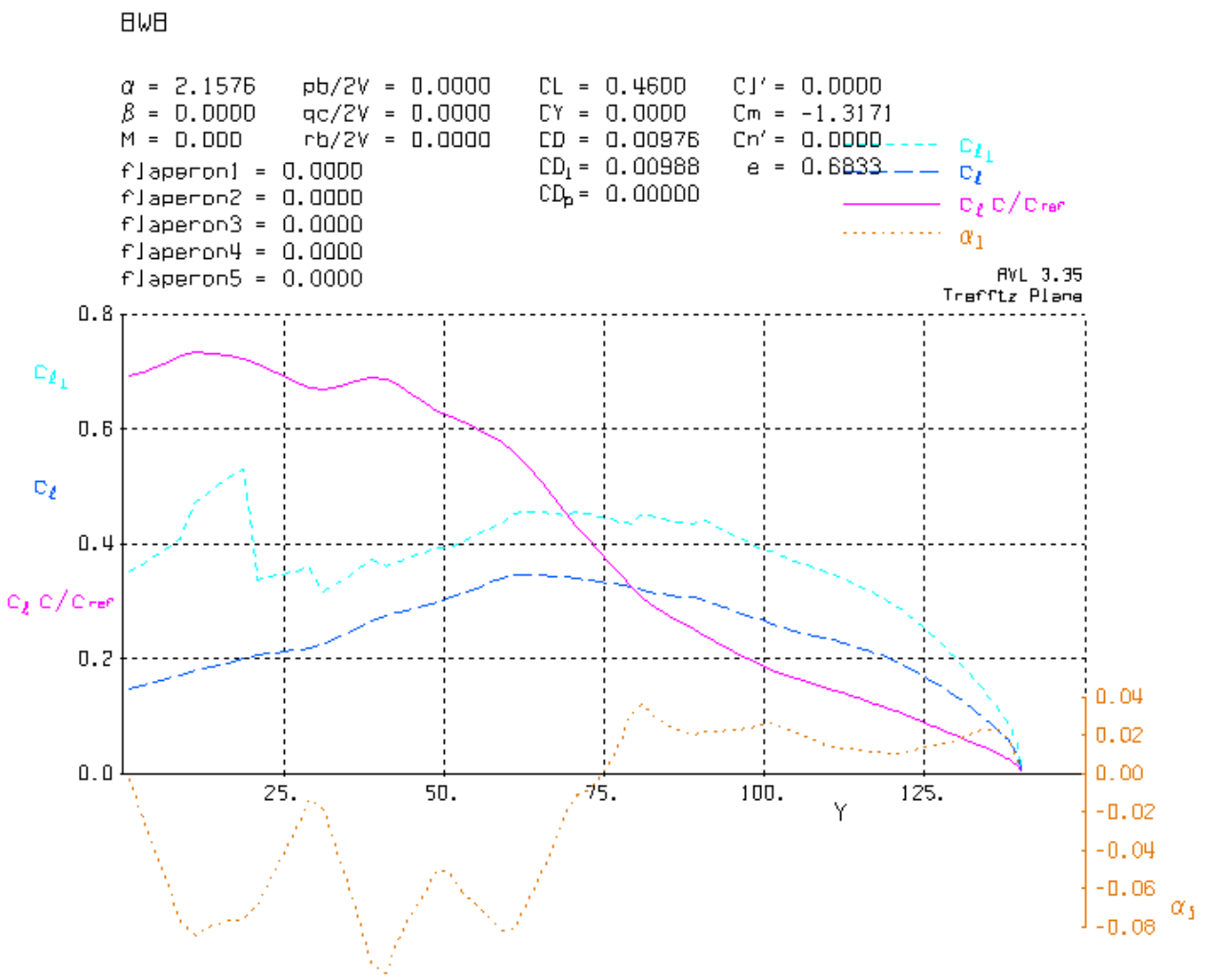

Figure 10: Trefftz Plot at Cruise Conditions

4 Approach and Stall Analysis: Nominal Geometry

In order to use AVL to estimate x_{ac}, x_{cp} and the static margin it is necessary to find constraints set out by being at approach and stall conditions.
We calculated the Mach numbers for approach and stall using an approach speed of 150kts as given by air traffic control; this is 0.227 times the speed of sound at this altitude. Given that the speed of approach is 1.3 times that of stall, the Mach number at stall is 0.174.

$$C_L = \frac{\text{Weight}}{q \cdot S_{ref}}$$

Since $L = W$, at sea level (where we will be landing), $\rho_\infty = 1.23 kg/m^3 = 0.00237 sl/ft^3$, U in ft/s and using $a = 1,120 ft/s$

$$q_{app} = 0.5 \rho_\infty U_{app}^2 = 76.0 \text{lbs}/ft^2$$

$$q_{stall} = 0.5 \rho_\infty U_{stall}^2 = 44.9 \text{lbs}/ft^2$$

$$\text{Weight} = W = W_{empty} + W_{payload} + 0.25 \cdot W_{fuel} = 650,000\text{lbs}$$

$$C_{L_{app}} = \frac{W}{q_{app} \cdot S_{ref}} = 1.09$$

$$C_{L_{stall}} = \frac{W}{q_{stall} \cdot S_{ref}} = 1.85$$

With the desired coefficient of lift and the required mach number, it is possible to use AVL to determine the aerodynamic center and the center of pressure; from which the stability margin can be calculated. AVL gives us the neutral point, x_{np}; which in this case is equivalent to the aerodynamic center because we have a tailless aircraft. To normalize this we simply divided by c_{mac}.

$$\frac{x_{ac}}{c_{mac}} = \frac{x_{np}}{c_{mac}}$$

Given that AVL gives us C_M at $x = 0$, the center of pressure may be found using the definition $x_{cp} = C_M/C_L$.

$$\frac{x_{cp}}{c_{mac}} = \frac{|C_M|}{|C_L|}$$

The stability margin is therefore $\frac{x_{ac}-x_{cp}}{c_{mac}}$, and in this normalized form, this value will simply need to be greater than 0.05 to meet the greater than 5% constraint.
We first ran an AVL simulation with no flaperon deflections and calculated the following values using $C_{mac} = 30.8$ ft.

$$\frac{x_{ac}}{c_{mac}} = 2.68$$

$$\frac{x_{cp}}{c_{mac}} = \frac{|C_M|}{|C_L|} = 2.77$$

This returns a stability margin of -0.0888 for approach conditions which is unstable.
Similarly for stall:

$$\frac{x_{ac}}{c_{mac}} = 2.59$$

$$\frac{x_{cp}}{c_{mac}} = \frac{|C_M|}{|C_L|} = 2.72$$

This returns a stability margin of -0.127 which is, again, unstable.
We figured that artificially reflexing the BWB with negative flaperon deflections might be helpful as this should create some pitch up moment; thus we put in negative flaperon deflections in order to generate some quasi-reflex.
After some trial and error, the following flaperon deflections were found to satisfy the stability conditions for both approach and stall:

Flaperon	1	2	3	4	5
Deflection (deg)	-25	-23	-20	-17	-15

With the aforementioned flaperon deflections at approach conditions:

$$x_{ac} = 2.67$$

$$x_{cp} = 2.39$$

This gives a static margin of 0.281 or 28.1% at approach conditions.
With the aforementioned flaperon deflections at stall conditions:

$$x_{ac} = 2.55$$

$$x_{cp} = 2.49$$

This gives a static margin of 0.0676 or 6.76% at stall conditions.
Included in figures X, X and X are plots of $c_l(y)$, $c_l(y)/c_{mac}$ for approach and then stall.

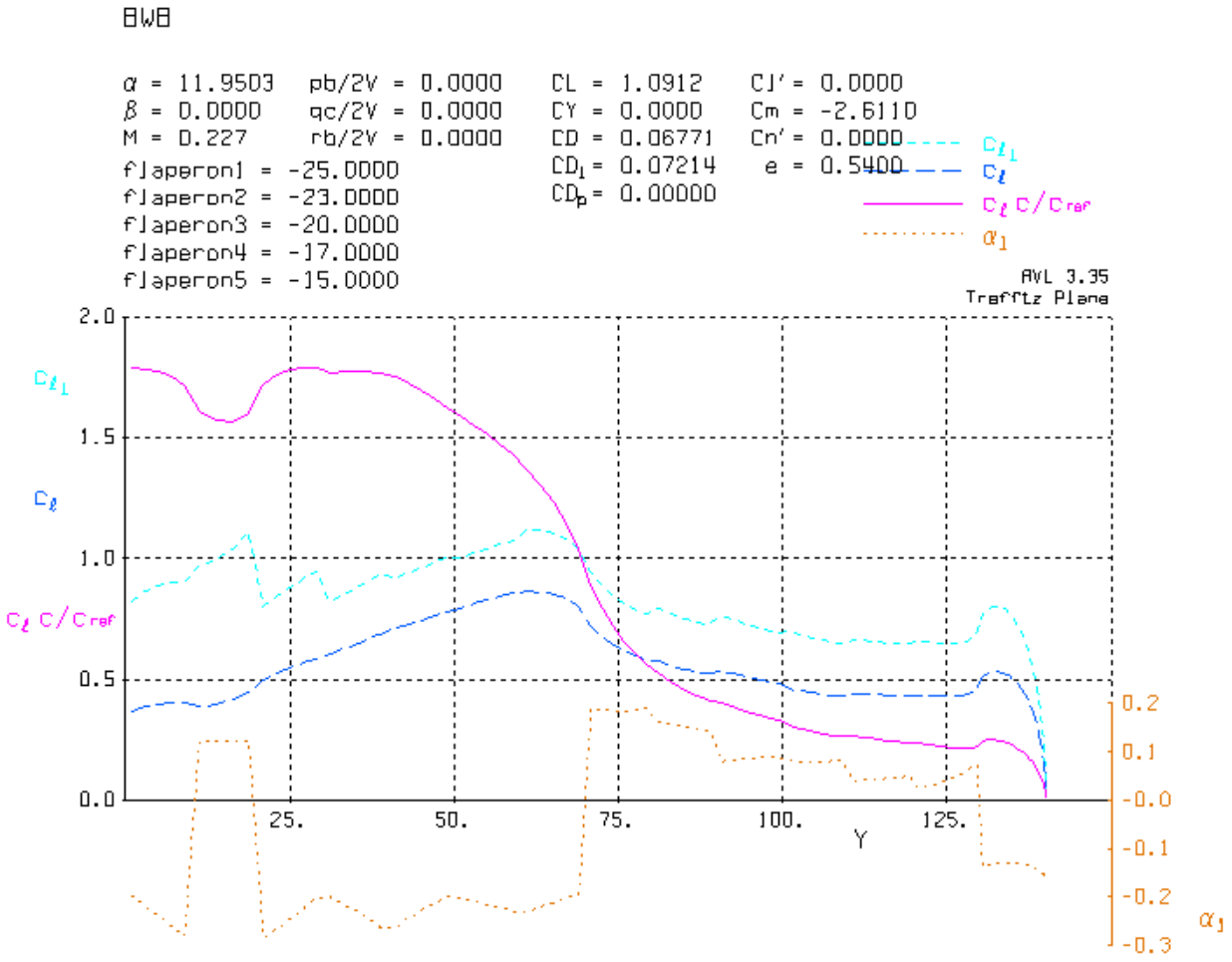

Figure 11: Trefftz Plot at Approach Conditions

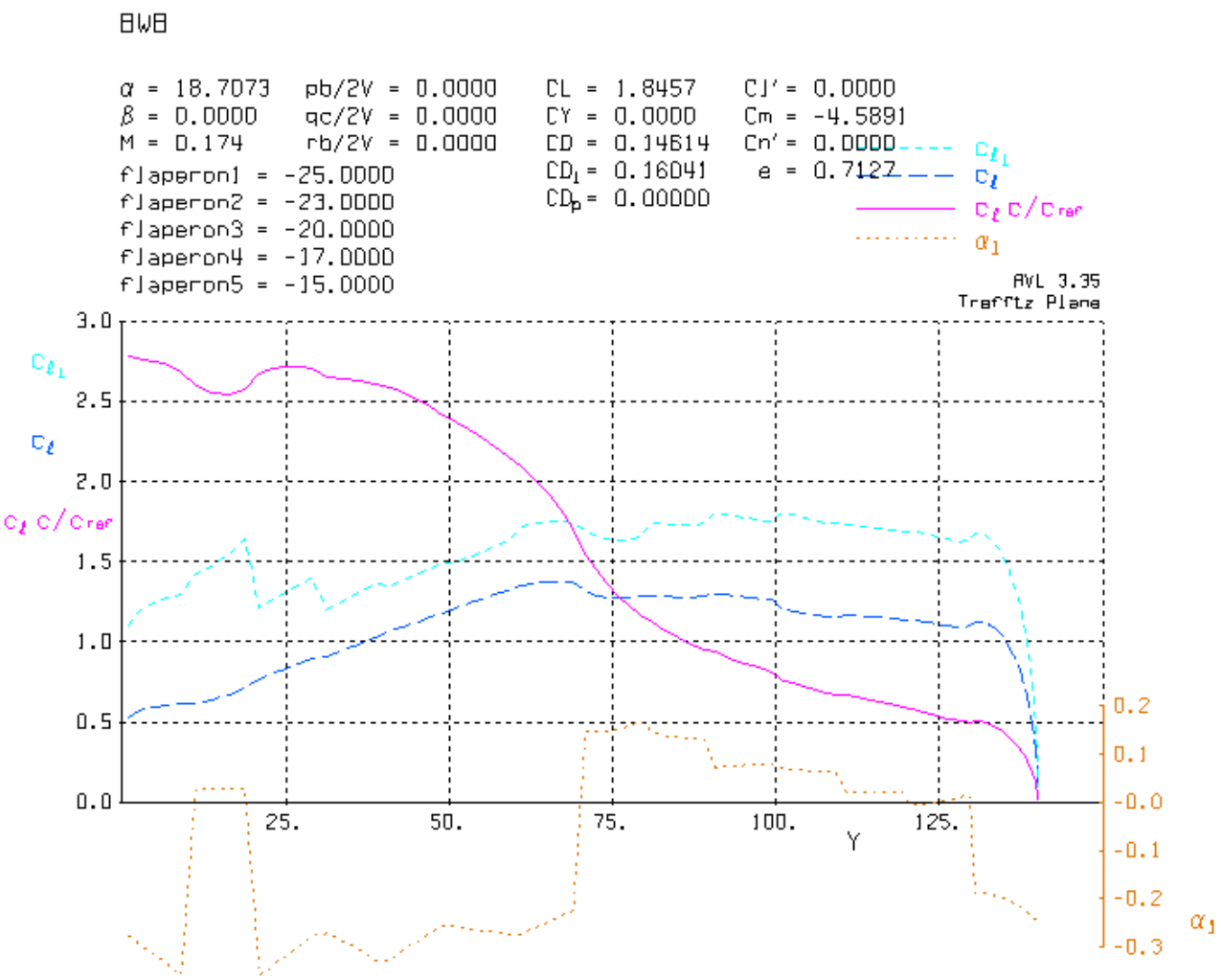

Figure 12: Trefftz Plot at Stall Conditions

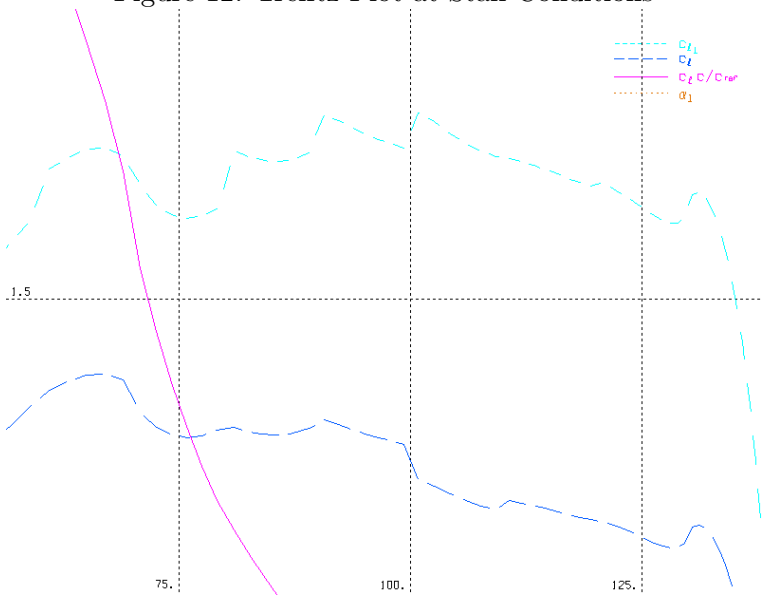

Figure 13: Close up at Stall Conditions

5 Redesign Strategy

The BWB is far from achieving the required stability at approach, stall and cruise conditions. Geometric modifications need to be made to restore the aircraft to a degree of positive pitch stability.

5.1 Reflex

Currently, the airplane has reflex on the trailing edge of the central airfoil sections to generate the pitch-down moment to stabilize the aircraft.
However, it is practically impossible to create supercritical reflexed airfoils because reflexed airfoils create a higher pressure region towards the trailing edge of the airfoil, causing a stronger shock. As a result, reflex will be chosen as one of the last methods of BWB modification, since the drag penalties are significant.

5.2 Chord Distribution

By making small modifications to the chord distribution, we can adjust the lift generated by different sections of the wing and affect the static margin of the aircraft. Most notably, we can couple increasing chord length of the tip sections with greater washout to get greater pitch-up moment due to increased negative lift at the wingtips.
We also need to make sure that the BWB has a relatively continuous chord distribution, for several reasons. Although the shape of the BWB essentially makes it impossible to violate the area rule, smoother changes in frontal cross-sectional area distribution will result in lower wave drag, and smoother changes in chord-wise area distribution will result in smoother sectional c_l distributions.

5.3 Geometric Twist

Greater washout will improve the static stability of the aircraft, but it has associated penalties with the induced drag and the lift generated by the aircraft due to the decrease in span efficiency.
Furthermore, modifying the effective angle of attack only provides advantages in certain flight regimes, and not others. For example, a twist distribution that was optimized for cruise may be suboptimal for approach and stall conditions. However, greater downwash at the wingtips is an effective way to decrease the pitch-down moment of the aircraft, lowering x_{cp} and improving the stability of the aircraft. It will play a critical role in the redesign strategy.

5.4 Sweep

We can take advantage of the negative lift generated at the wingtips of the BWB to provide a pitch-up moment and move the center of pressure of the aircraft closer towards the nose, improving its static margin. However, there are other tradeoffs associated with sweep, such as an increase in the sectional c_l towards the wingtips, which may require the addition of extra washout. Also, high lift devices are less effective on highly swept wings compared to unswept wings.
Increasing the sweep has the added benefit of significantly reducing wave drag. Since most other modifications to the aircraft are prone to decreasing span efficiency and increasing the drag, coupling an increase in sweep with other geometry modification methods seems effective.

6 Final Design

6.1 Airplane Modification Framework

A MATLAB code was generated to be able to directly input changes in chord distribution, in sweep, in geometric twist and in dihedral angle into the original BWB geometry. All modifications were made as a fraction of the original BWB parameters (for example, the chord was scaled by 1.1, or the sweep was increased to 125% of original values etc.) This allowed us to make quick geometry modifications to be able to obtain the desired stability margin during all three flight conditions (approach, stall, and cruise).

6.2 Proposed Plan of Action

The sweep, geometric twist and the chord length distribution of the wing will be modified to make the aircraft stable in cruise conditions.
We will start by increasing the sweep of the wing by 15% of its original value. Both the x_{cp} and the x_{ac} would be predicted to increase, and the change would confer a small increase in the static margin of the system.
Afterwards, we will add greater washout at the wingtips to decrease the pitch-down moment at the nose, and move the x_{cp} towards the nose.
This will be followed by an increase in the chord length of the body sections to generate more lift in the center-body, decreasing the lift coefficient towards to wingtips to achieve an improvement in the span efficiency.
Once a stable configuration is determined, the appropriate flaperon deflections will be found to make the redesigned geometry stable at approach and stall conditions.

6.3 Sweep Modification

15% extra sweep was added to the model. Using AVL, we found the following values for x_{cp} and x_{ac} at cruise:

$$\frac{x_{cp}}{c_{mac}} = 3.17$$
$$\frac{x_{ac}}{c_{mac}} = 3.04$$

Therefore, our stability margin (SM) is -13.4% and the span efficiency, $e = 0.690$.
As expected, the extra sweep moved both x_{cp} and x_{ac} away from the nose, but improved the overall stability of the aircraft. It was also surprising that the span efficiency of the aircraft increased slightly.

6.4 Twist Modification

Initially, only the four wingtip sections were given 3 degrees of washout to achieve a stability margin of -4.70%. The large increase in static stability ($\tilde{9}$%) was achieved through the negative lift generated by the wingtips.
It was observed subsequently that the sectional lift coefficient of the body was significantly lower than the c_l near the wingtips. This means that the airplane could use an improvement in stall characteristics by having higher sectional c_ls near the fuselage, so that the airplane does not lose roll control when in stall. As a result, the middle 4 airfoil sections were given 3 degrees of positive angle of attack. This further increased the stability margin, to yield the results below:

$$\frac{x_{cp}}{c_{mac}} = 2.91$$
$$\frac{x_{ac}}{c_{mac}} = 3.05$$

The Stability margin is 13.1%, and span efficiency, $e = 0.479$.
We have achieved the stability margin, but with a drastic span efficiency penalty. As a result, we found it appropriate to do some fine tuning on the BWB parameters and converge on a final design that compromises between static stability and span efficiency.

6.5 Chord Modification

We incorporated an increase in the chord length of the body sections to increase lift in those sections and to decrease the c_l of the outboard sections. We also smoothed out the geometric twist distribution to obtain a smoother lift distribution. There were seven separate design iterations in the process of converging to a final design, but for the interests of this report only the final design will be presented.

6.6 Final Geometry

Sweep	1.15														
Chord # from center	1	2	3	4	5	6	7	8	9	10	11	12	13	14	15
Chord length	1.075	1.05	1.025	1.0	1	1	1	1	1	1	1	1	1	1	1
Geometric twist	4	3	2	1.5	1	0.5	0	0	0	0	0	-0.5	-1	-1.5	-2.75

The sweep and the chord length are given as a fraction of the respective nominal geometry values. The geometric twist given in degrees.

Original BWB Flaperons

Flaperon	1	2	3	4	5
Position (x/c)	0.9	0.7	0.7	0.7	0.7
Position (y)	10-30	70-90	90-110	110-120	120-130

Redesigned BWB Flaperons

Flaperon	1	2	3	4	5
Position (x/c)	0.9	0.7	0.7	0.7	0.7
Position (y)	10-30	70-90	90-110	110-120	120-130

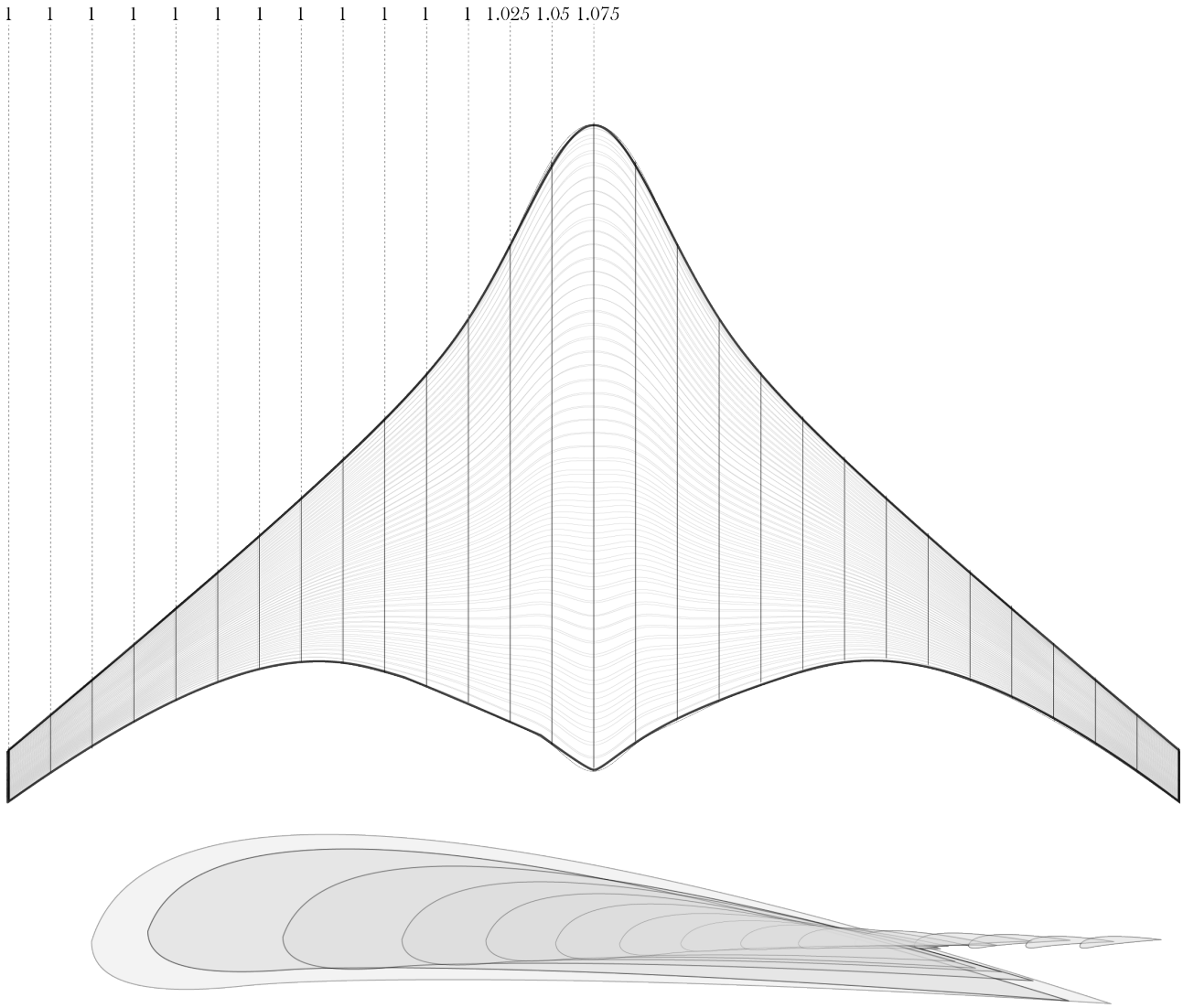

Figure 14: Diagram to show Final Geometry

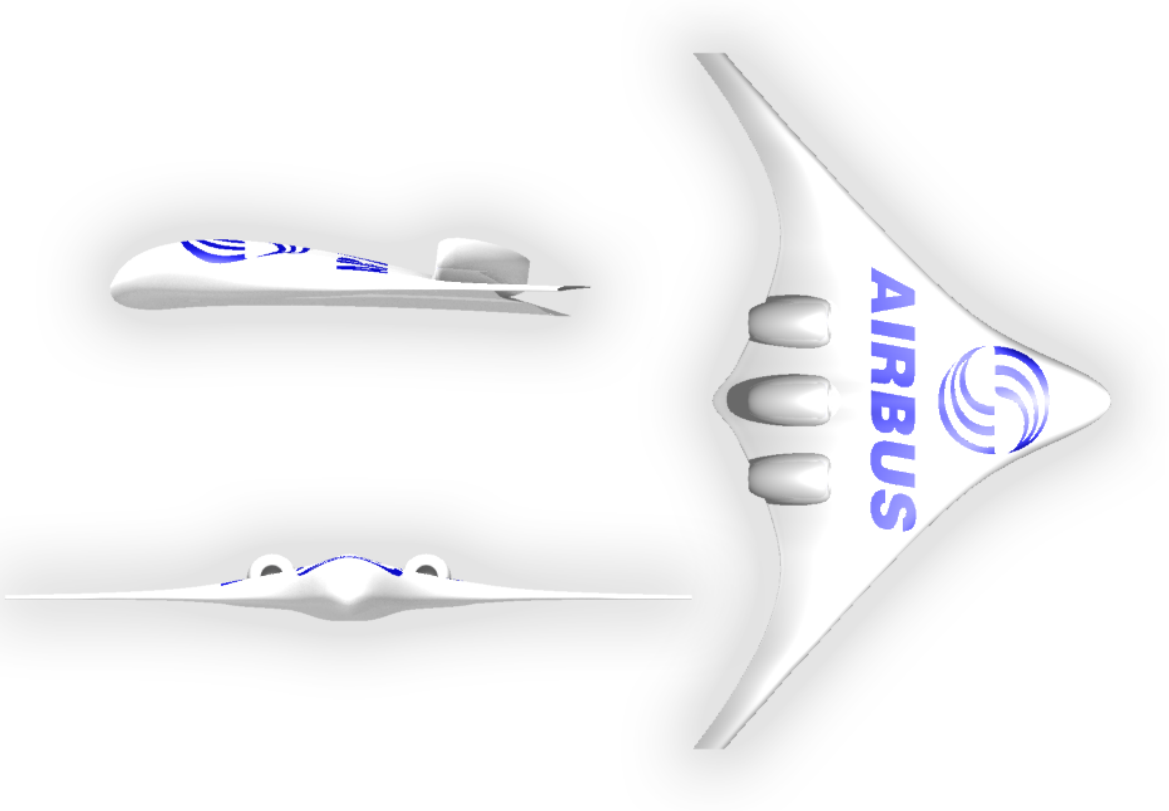

Figure 15: Renders of Final Geometry, Plan, Elevation and Section

7 Final Design Analysis

7.1 Cruise Analysis

In the cruise analysis, the reference area and mean aerodynamic chord were assumed to have not changed significantly, thus the same values for both these parameters were used. It is of note that, S_{ref} was analytically computed to be about 100 square feet more.
Much the same as with the nominal geometry except with the sweep angle increased by 15.0%, wave drag was calculated to be:

$$C_{D_{wave}} = 0.00700$$

Again, induced drag and drag were computed with the use of AVL the same way as for the nominal geometry:

$$C_D = 0.0125$$

$$C_{D_i} = 0.0128$$

This gives a final $C_{D_{tot}} = 0.0323$ and thus a final value of drag of $56,500$lbs.
x_{cp}, x_{ac} and the stability margin were calculated the same way that is outlined above:

$$\frac{x_{ac}}{c_{mac}} = 3.05$$

$$\frac{x_{cp}}{c_{mac}} = 3.00$$

Which gives a stability margin of 0.0500 or 5%, which only just meets the requirement.

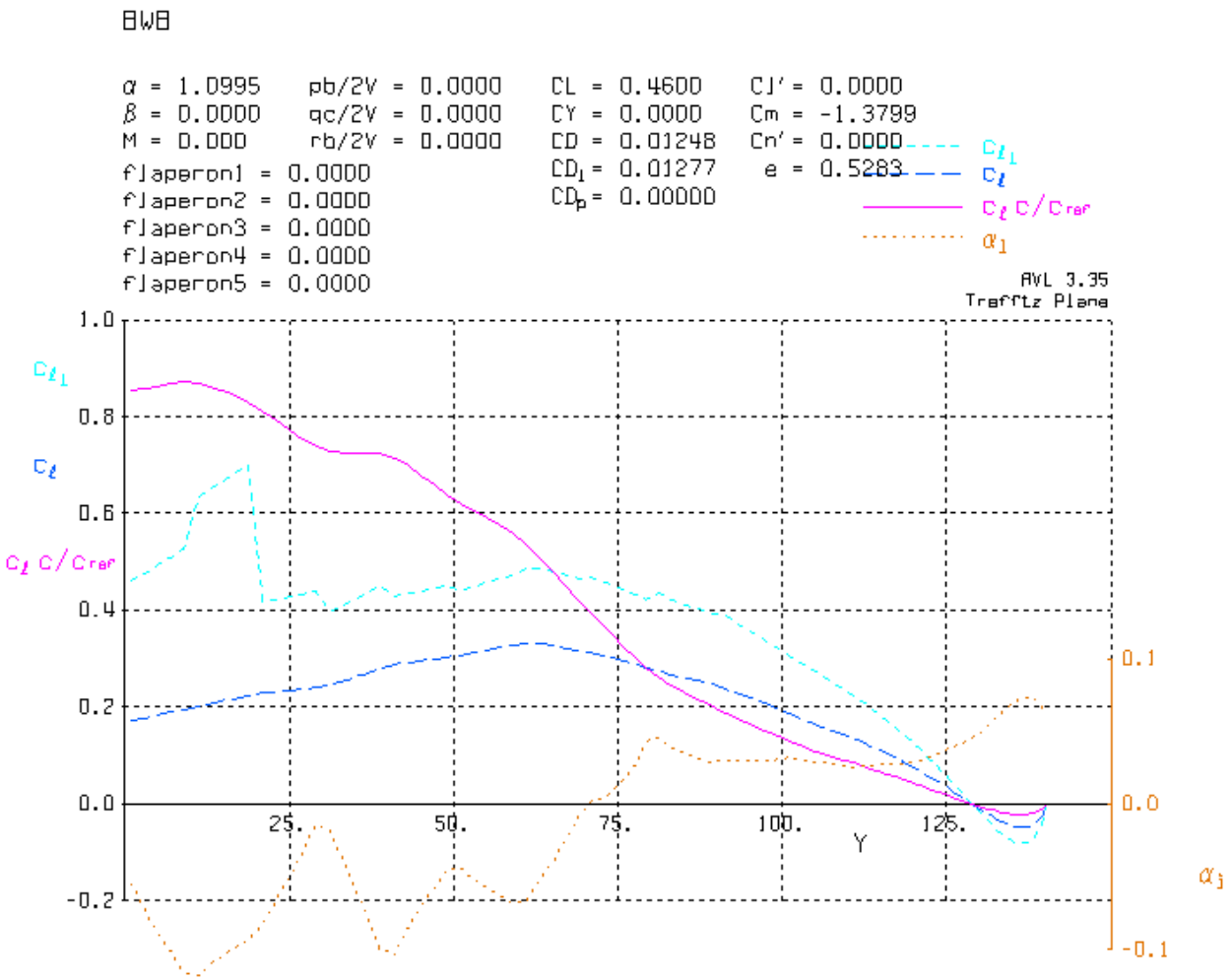

Figure 16: Trefftz Plot at Cruise Conditions for Redesigned BWB

7.2 Approach and Stall Analysis

In approach and stall analyses, the same method was used as with the nominal geometry, however with the modification of the increased reference area, $S_{ref} = 8210 ft^2$. This value was computed using a trapezoidal approximation. We used AVL to model the impact of flaperon deflection and have used its convention of denoting downward deflection as positive. An initial flaperon deflection of -15 degrees for all flaperons was used and was found to satisfy both approach and stall conditions.
At a -15 degree deflection for all flaperons, the following conditions for approach were found.

$$\frac{x_{ac}}{c_{mac}} = 3.05$$

$$\frac{x_{cp}}{c_{mac}} = 2.74$$

With a stability margin of 0.300, or 30.0% which far exceeds the 5.00% target.

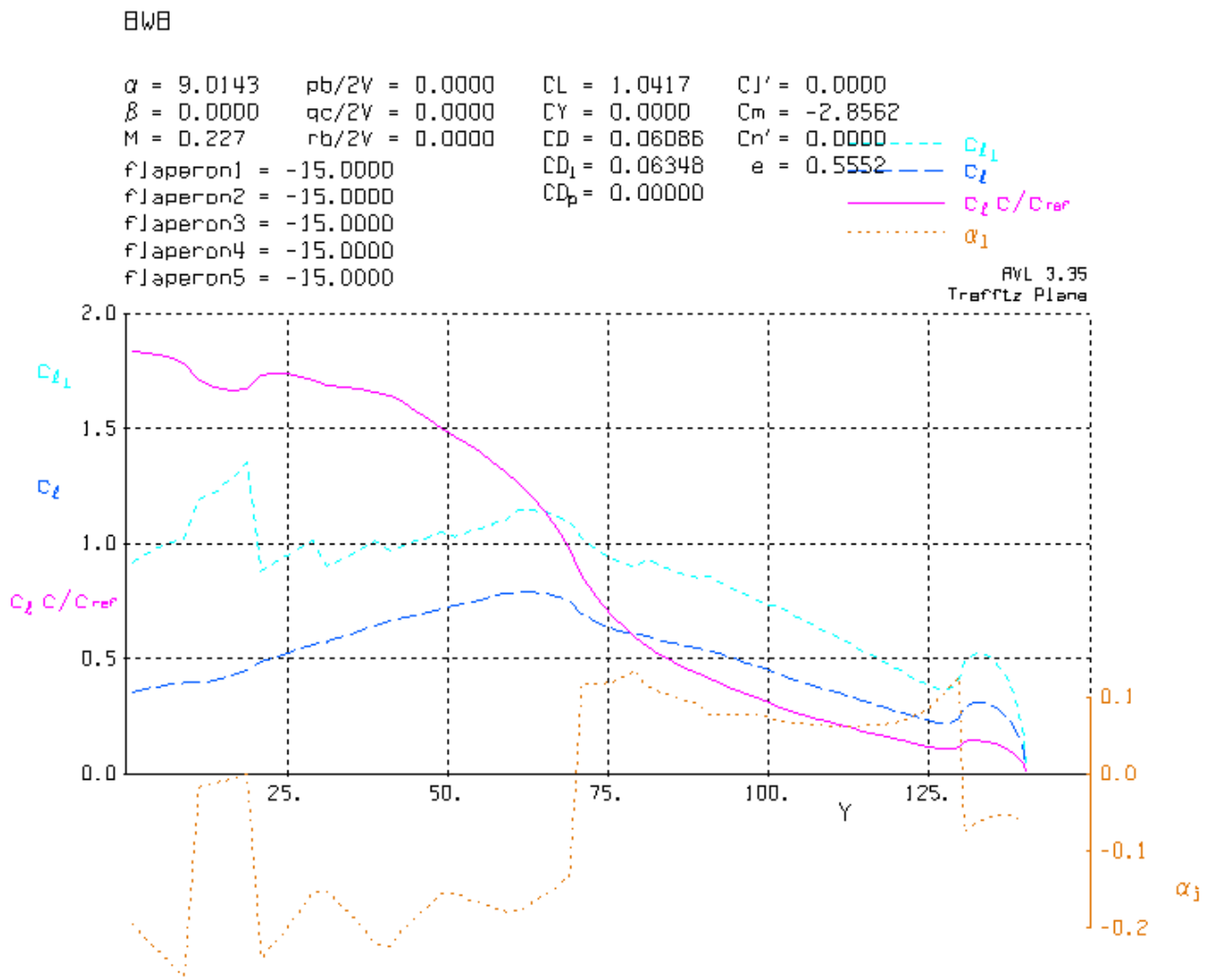

Figure 17: Trefftz Plot at Approach Conditions for Redesigned BWB

At a -15 degree deflection for all flaperons, the following conditions for stall were found.

$$x_{ac} = 2.93$$

$$x_{cp} = 2.85$$

With a stability margin of 0.0816, or 8.16% which slightly exceeds the 5.00% target.

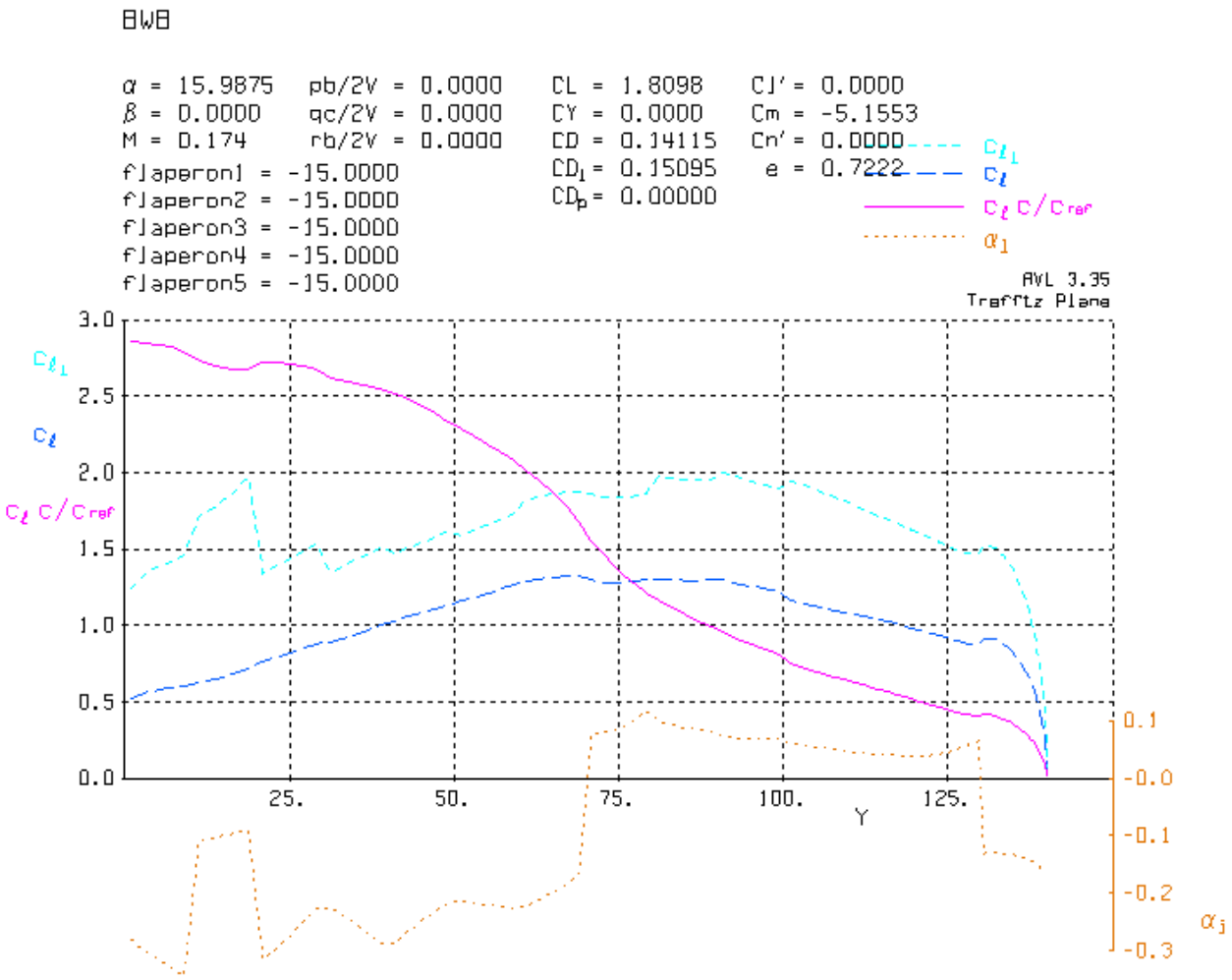

Figure 18: Trefftz Plot at Stall Conditions for the Redesigned BWB

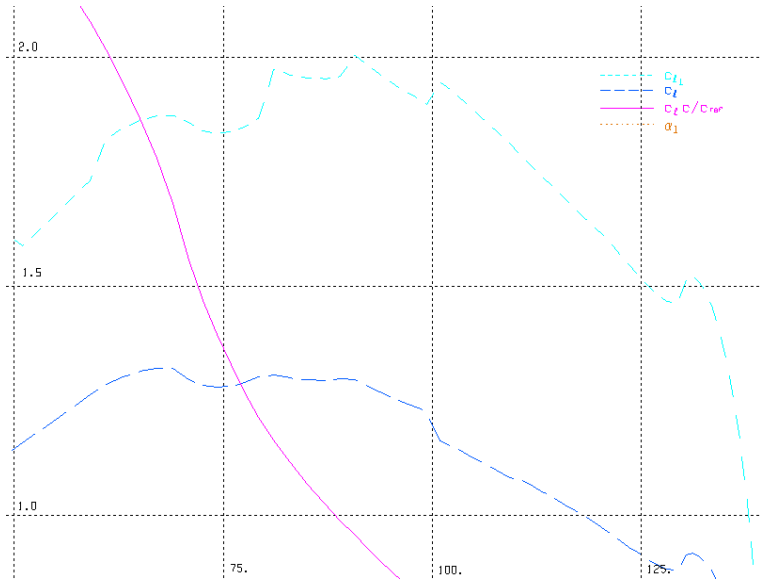

Figure 19: Trefftz Plot zoomed in for Stall Conditions

8 Review

Please note that this design is far from optimal. It is one of the many designs in the incredible configuration space that satisfies the design requirements. First of all, the stall characteristics have to be improved by further increasing the sectional c_l of the body.
Furthermore, it is more than likely that there are more favorable design modifications involving chord distribution, sweep, geometric twist and the many other parameters that we have not considered in achieving the required stability margin. However, in our analyses, we have managed to redesign the BWB to have a 5% static margin with a minimal drag penalty.

References

[1] R. H. Liebeck, *Design of the Blended Wing Body Subsonic Transport*. 2004.

[2] O. Gur, W. H. Mason and J. A. Schetz, *Full Configuration Drag Estimation*. 2009.

[3] J. D. Cole and N. D. Malmuth, *Wave drag due to lift for transonic airplanes*. 2004.

[4] W.H. Mason, *Transonic Aerodynamics of Airfoils and Wings*. 2006.

[5] M. Drela, *Flight Vehicle Aerodynamics*. 2013.

[6] M. Drela *Athena Vortex Lattice*. 2010: `http://web.mit.edu/drela/Public/web/avl/`

[7] Wikipedia *Vortex Lattice Method*: `http://en.wikipedia.org/wiki/Vortex_lattice_method`